



**HAL**  
open science

## Viscosity of Liquid Fayalite up to 9 GPa

Holly Spice, Chrystèle Sanloup, Benjamin Cochain, Charlotte de Grouchy,  
Yoshio Kono

► **To cite this version:**

Holly Spice, Chrystèle Sanloup, Benjamin Cochain, Charlotte de Grouchy, Yoshio Kono. Viscosity of Liquid Fayalite up to 9 GPa. *Geochimica et Cosmochimica Acta*, 2015, 148, pp.219-227. 10.1016/j.gca.2014.09.022 . hal-01105412

**HAL Id: hal-01105412**

**<https://hal.science/hal-01105412>**

Submitted on 20 Jan 2015

**HAL** is a multi-disciplinary open access archive for the deposit and dissemination of scientific research documents, whether they are published or not. The documents may come from teaching and research institutions in France or abroad, or from public or private research centers.

L'archive ouverte pluridisciplinaire **HAL**, est destinée au dépôt et à la diffusion de documents scientifiques de niveau recherche, publiés ou non, émanant des établissements d'enseignement et de recherche français ou étrangers, des laboratoires publics ou privés.

# 1 Viscosity of Liquid Fayalite up to 9 GPa

2 Holly Spice<sup>1\*</sup>, Chrystèle Sanloup<sup>1,2</sup>, Benjamin Cochain<sup>1</sup>, Charlotte de  
3 Grouchy<sup>1</sup>, Yoshio Kono<sup>3</sup>

4 <sup>1</sup>*Scottish Universities Physics Alliance (SUPA), and Centre for Science at Extreme*  
5 *Conditions, School of Physics and Astronomy, University of Edinburgh, Edinburgh, EH9*  
6 *3JZ, UK*

7 <sup>2</sup>*Sorbonne Universités, UPMC Univ Paris 06, UMR 7193, ISTEP, F-75005 Paris,*  
8 *France*

9 <sup>3</sup>*HPCAT, Geophysical Laboratory, Carnegie Institution of Washington, USA*

---

## 10 Abstract

The viscosity of liquid fayalite ( $\text{Fe}_2\text{SiO}_4$ ) was determined up to 9.2 GPa and 1850 °C using *in situ* falling sphere viscometry and X-ray radiography imaging. The viscosity of liquid fayalite was found to decrease with pressure, reducing by a factor of 2.5 between ambient pressure and 9.2 GPa. The results are in contrast with previous studies on depolymerised silicate melts which found viscosity to increase with pressure. In accordance with recent *in situ* structural measurements on liquid fayalite, the viscosity decrease is likely a result of the increase in Fe-O coordination with pressure. In addition, temperature is found to have little effect on the viscosity at high pressure. The results show that liquid silicate viscosities need to be considered on an individual basis and can be strongly dependent on the melt structure and composition. This has important implications for models of planetary differentiation. In particular, terrestrial bodies with high Fe contents and reducing mantle conditions are likely to have had very mobile melts at depth.

## 11 **1. Introduction**

12 The viscosity of liquid silicates (i.e. magmas) is a fundamental property  
13 that influences igneous processes, as it controls the transport properties of  
14 magmas in planetary interiors. As such, viscosity of liquid silicates will have  
15 been an important controlling factor in influencing the formation of the ter-  
16 restrial planets during the existence of the potential magma oceans. Many of  
17 the previous studies on silicate melt viscosity at high pressure were carried  
18 out on aluminosilicate melts e.g. basalt and andesite (Kushiro et al., 1976),  
19 jadeite (Kushiro, 1976; Suzuki et al., 2011), and albite (Suzuki et al., 2002).  
20 Viscosity was found to decrease significantly with increasing pressure in these  
21 melts.

22 Despite its importance for magma ocean systems, the viscosity of depoly-  
23 merised silicate melts at high pressure has not been extensively studied due  
24 to experimental difficulties, including high melting temperatures and very  
25 low melt viscosities. Liquid diopside ( $\text{CaMgSi}_2\text{O}_6$ ) (Brearley et al., 1986;  
26 Taniguchi, 1992; Reid et al., 2003) and peridotite (Liebske et al., 2005) are  
27 the only depolymerised silicate melt viscosities determined experimentally  
28 so far. The viscosity of these liquids was found to initially increase with  
29 pressure, but decrease above  $\sim 9\text{-}10$  GPa.

30 It is also important to investigate the physical properties of iron-rich  
31 liquid silicates because the FeO content of the planets is highly variable,  
32 estimated to range from 3 wt% in Mercury's mantle (Robinson and Taylor,  
33 2001), to 22 wt% in the lunar and martian mantles (Cahill et al., 2009; Bara-  
34 toux et al., 2011). This may lead to important differences in the processes  
35 occurring in the respective magma oceans of planets. In addition, Fe can ex-

36 ist in different oxidation states (2+, 3+) which has been shown to influence  
37 silicate melt viscosity e.g. (Liebske et al., 2003; Bouhifd et al., 2004; Chevrel  
38 et al., 2014). Additionally, there is no data for depolymerised, low viscosity  
39 Fe-rich liquids, and computational methods have only investigated Mg-rich  
40 liquid viscosities such as  $\text{MgSiO}_3$  (Karki and Stixrude, 2010) and  $\text{Mg}_2\text{SiO}_4$   
41 (Ghosh and Karki, 2011). Therefore, experimental determination of high-P  
42 physical properties of such Fe-rich liquids is required.

43 Here we present viscosity experiments carried out on the molten iron-rich  
44 end member of olivine, fayalite ( $\text{Fe}_2\text{SiO}_4$ ), a highly depolymerised silicate,  
45 up to 9.2 GPa. The results are discussed by comparison with recent *in situ*  
46 structural measurements (Sanloup et al., 2013a) in order to determine the  
47 relationship between the melt structure and viscosity at high pressure.

## 48 **2. Experimental Methods**

### 49 *2.1. High pressure techniques*

50 Experiments on molten fayalite up to 9.2(6) GPa and 1850(95) °C were  
51 performed using a Paris-Edinburgh press. Natural fayalite supplied by Alfa  
52 Aesar was powdered and packed inside a graphite capsule. The cell-assembly  
53 (Sakamaki et al., 2012; Sanloup et al., 2013a) shown in Fig. 1, is optimized  
54 to allow a large vertical access to the sample and to limit the extrusion of  
55 cell materials, even at high  $P$ - $T$  conditions. The cell design uses low density  
56 materials such as boron epoxy and graphite to allow maximum transparency  
57 for X-rays. Zirconia was used for thermal insulation and to stabilise the  
58 cell. MgO caps + packed pyrex powder were inserted above and below the  
59 graphite capsule in order to prevent the oxidation of iron and the consequen-

60 tial decomposition of fayalite at high  $T$  (Sanloup et al., 2013a). A rhenium  
61 sphere was inserted at the top of each capsule to enable it to fall through  
62 the sample upon melting. To enable proper falling, a thin layer of sample  
63 was inserted to cover the sphere. The pressure was determined from the  
64 cell-volume of the MgO ring pressure-transmitting medium, which uses the  
65  $P$ - $V$ - $T$  relation of MgO derived by simultaneous elastic wave velocity and *in*  
66 *situ* X-ray measurements by Kono et al. (2010) and accounts for the pressure  
67 difference between the sample and the MgO ring. X-ray diffraction patterns  
68 of the MgO pressure-transmitting medium were collected at 100 °C below  
69 the liquidus and after the spheres had fallen to determine the pressure. The  
70 temperature was determined from previous calibration measurements of the  
71 cell-assembly (Kono et al., 2014).

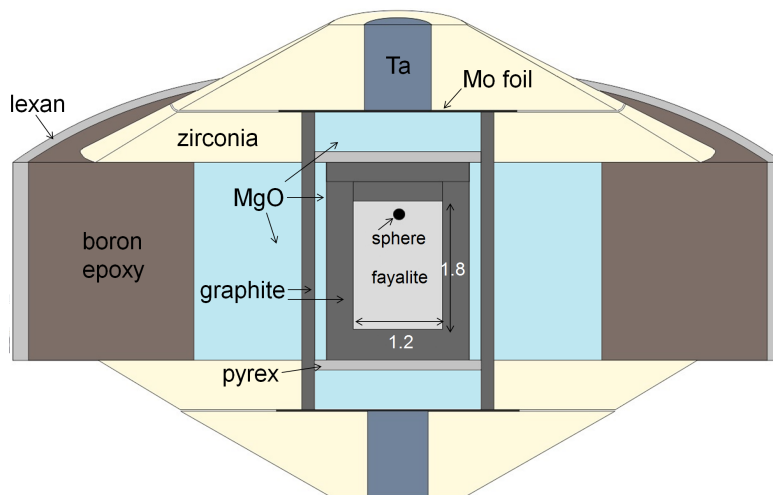


Figure 1: Schematic cross section of the cell assembly; adapted from Sakamaki et al. (2012). Dimensions are given in mm.

72 *2.2. Viscosity measurements*

73 High pressure falling sphere viscometry, in combination with *in situ* X-ray  
 74 imaging (Kono et al., 2013), was carried out at beamline 16-BM-B, High Pres-  
 75 sure Collaborative Access Team (HPCAT) at the Advanced Photon Source,  
 76 Argonne National Laboratory, USA. The sample was pressurised at room  
 77 temperature and the temperature was then gradually raised to approximately  
 78 100 °C below the liquidus. The sample was then rapidly heated to a super-  
 79 liquidus set-point temperature, until either melting or the target  $T$  of 1600 °C  
 80 was achieved. The difference between the X-ray absorption coefficients of the  
 81 rhenium sphere and silicate melt allows for clear imaging of the sphere falling  
 82 through the melt. The viscosity of liquid fayalite is extremely low, therefore  
 83 a high speed video camera (Photron FASTCAM SA3) was used to collect  
 84 images of the falling spheres at a rate of 250 frames per second. The imaged  
 85 descent path of the sphere was used to calculate a distance/time curve, from  
 86 which it is possible to calculate the terminal velocity  $v_s$  of the sphere. The  
 87 viscosity  $\eta$  of the liquid can then be calculated using Stokes law:

$$\eta = \frac{2gr_s^2(\rho_s - \rho_l)W}{9v_sE} \quad (1)$$

88 where  $r_s$  is the radius of the sphere,  $\rho_s$  and  $\rho_l$  are the densities of the sphere  
 89 and the liquid respectively at a given pressure and temperature, and  $g=9.803$   
 90  $\text{m}\cdot\text{s}^{-2}$  is the acceleration due to gravity.  $W$  and  $E$  are correction factors that  
 91 account for the wall and end-effects of a finite cylindrical container (Faxén,  
 92 1922) of radius  $r_c$  and height  $h_c$  are given by:

$$W = 1 - 2.104 \left(\frac{r_s}{r_c}\right) + 2.09 \left(\frac{r_s}{r_c}\right)^3 - 0.95 \left(\frac{r_s}{r_c}\right)^5 \quad (2)$$

$$E = 1 + 3.3 \left( \frac{r_s}{h_c} \right) \quad (3)$$

93 The radii  $r_s$  of the rhenium spheres, as determined from X-ray shadow-  
 94 graph images using the high resolution camera, ranged between 54-93  $\mu\text{m}$ ,  
 95 where the largest uncertainty was  $\pm 2 \mu\text{m}$ . The density of the spheres was  
 96 calculated using the third-order Birch-Murnaghan equation of state, account-  
 97 ing for the thermal expansion of rhenium ( $6.63 \times 10^{-6} \text{ K}^{-1}$ ), using data from  
 98 Vohra et al. (1987). The density of liquid  $\text{Fe}_2\text{SiO}_4$  at high pressure was taken  
 99 from Sanloup et al. (2013a) who determined the density of liquid fayalite  
 100 at  $1627^\circ\text{C}$  up to 7.5 GPa. These measurements were in good agreement  
 101 with Thomas et al. (2012) who determined the density of fayalite liquid us-  
 102 ing shock wave, sink/float and ultrasonic experiments and with shock wave  
 103 experiments carried out by Chen et al. (2002). For experimental runs not  
 104 carried out at  $1627^\circ\text{C}$ , thermal expansion was accounted for using a thermal  
 105 expansion coefficient of  $4.8 \times 10^{-5} \text{ K}^{-1}$  (Agee, 1992).

106 The maximum uncertainty in  $P$  and  $T$  was  $\pm 0.6 \text{ GPa}$  and  $\pm 95^\circ\text{C}$ , re-  
 107 spectively. The  $P$  uncertainty resulted in an uncertainty in the determination  
 108 of the liquid and rhenium sphere density at high pressure. The largest error  
 109 in the liquid density was 1.5%, while the largest error in the sphere density  
 110 was 1.1%, and are therefore relatively minor. Due to the small sphere size  
 111 used in our study, the uncertainty in the measurement of the sphere radii  
 112 also contributes to the overall viscosity uncertainty. The high-resolution X-  
 113 ray radiography set-up had an image resolution of  $\pm 2 \mu\text{m}$ .(Kono et al.,  
 114 2014).

115 However, it is the uncertainty in the terminal velocity determination

116 that plays the dominant role in the precision of the viscosity measurements  
117 (Brizard et al., 2005). In this study, the terminal velocities were determined  
118 with standard deviations of  $\pm 2\text{-}6\%$ . In addition, an error in terminal veloc-  
119 ity may arise if the shape of the sphere deviates from spherical. The actual  
120 terminal velocity of an ellipsoid particle ( $v_e$ ) may be found by multiplying  $v_s$   
121 by a shape factor  $S$  (Kerr and Lister, 1991). Our most elliptical sphere had  
122 an aspect ratio of  $c/a = 0.85$ , which corresponds to a shape factor of 0.998  
123 and thus a 0.2% error in the terminal velocity calculation. Indeed, the effect  
124 of an elliptical shape is small even at  $c/a = 0.5$ , which results in  $S = 0.96$ ,  
125 thus corresponding to only a 4% error in terminal velocity. Therefore, the  
126 effect of sphere shape in our study can be considered to be negligible on the  
127 final viscosity result. The overall uncertainty in the final viscosity values,  
128 determined by standard error propagation, was  $<10\%$ .

### 129 **3. Results**

#### 130 *3.1. Fayalite liquid viscosity*

131 The experimental conditions, sphere diameter ( $d_s$ ), terminal velocity and  
132 viscosity results are presented in Table 2.

133 X-ray shadowgraph images of the rhenium sphere falling during one of  
134 the experimental runs (Run B13, 5.1 GPa, 1650 °C) are shown in Fig. 2a.  
135 A plot of the sphere falling distance against time for this run is shown in  
136 Fig. 2b. The points show a good fit to the straight line, indicating that the  
137 sphere reached a constant terminal velocity after an initial acceleration. The  
138 velocity/time plot for the rhenium sphere of experiment B13 is shown in Fig.  
139 2c. After the initial acceleration, the sphere reaches a “velocity plateau”,

<i>Run</i>	<i>P</i> GPa	<i>T</i> °C	<i>d<sub>s</sub></i> μm	<i>v<sub>s</sub></i> mm·s <sup>-1</sup>	<i>η</i> mPa·s
A5	2.0 ± 0.5	1350 ± 70	173 ± 2	3.7 ± 0.1	51.8 ± 2.8
A10	3.6 ± 0.5	1550 ± 80	171 ± 2	5.1 ± 0.2	37.9 ± 3.6
A12	6.3 ± 0.5	1600 ± 80	185 ± 2	6.4 ± 0.2	34.3 ± 2.6
A8	9.2 ± 0.6	1850 ± 95	185 ± 2	7.2 ± 0.1	30.7 ± 2.6
B17	1.3 ± 0.5	1580 ± 80	183 ± 2	4.0 ± 0.2	51.4 ± 4.0
B14	2.8 ± 0.5	1570 ± 80	155 ± 2	4.0 ± 0.2	41.5 ± 3.7
B11	3.8 ± 0.5	1600 ± 80	133 ± 2	3.2 ± 0.1	40.5 ± 2.7
B7	4.3 ± 0.5	1640 ± 80	108 ± 2	2.3 ± 0.1	40.4 ± 3.6
B13	5.1 ± 0.5	1650 ± 85	173 ± 2	5.3 ± 0.2	37.1 ± 2.3

Table 1: Experimental run conditions, results and uncertainties

140 where the sphere is deemed to have reached its terminal velocity.

141 The viscosity of liquid fayalite decreased along the liquidus (Run A) from  
142  $76.0 \pm 6.7$  mPa·s at ambient pressure, 1250 °C (Shiraishi et al., 1978), to  
143  $30.7 \pm 2.6$  mPa·s at 9.2 GPa, 1850 °C (Fig. 3a and 3b). Viscosity decreased  
144 rapidly from ambient pressure to around 4 GPa, after which it decreased  
145 much more slowly. In order to confirm that the viscosity decrease was due  
146 to increasing pressure and not increasing temperature, the viscosity of liquid  
147 fayalite was measured as a function of pressure along the 1600 °C isotherm,  
148 within  $\pm 50$  °C (Run B). At 1600 °C, the viscosity of liquid fayalite decreased  
149 from  $51.4 \pm 4.0$  mPa·s at 1.3 GPa, to  $34.3 \pm 2.6$  mPa·s at 6.3 GPa (Fig. 3a),  
150 suggesting that increasing pressure is indeed the main cause of the viscosity  
151 decrease along the fayalite liquidus.

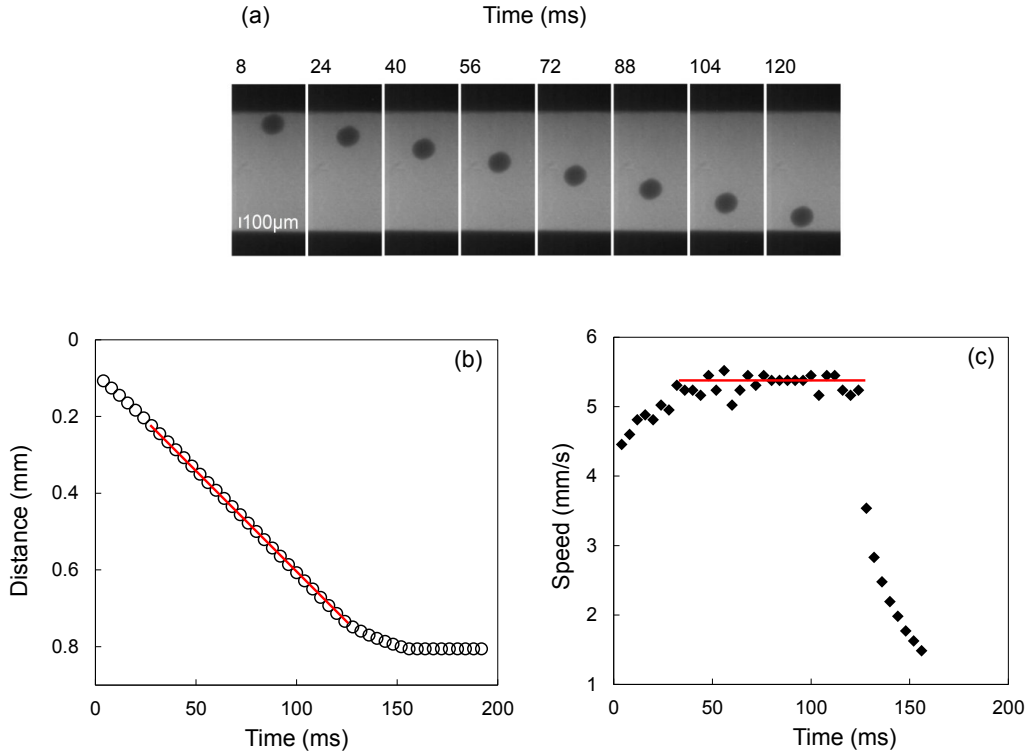


Figure 2: (a) A series of X-ray radiography images showing the rhenium sphere (radius  $86.5 \mu\text{m}$ ) descent through liquid  $\text{Fe}_2\text{SiO}_4$  from experiment B13 at 5.1 GPa and  $1650^\circ\text{C}$ . Every 4th frame is shown between 8 and 120 ms. (b) The results of the sphere fall analysis for each frame during experiment B13. The points show a good fit to a straight line and the constant gradient before the sphere reaches the bottom of the capsule indicates that terminal velocity was achieved. (c) The velocity/time plot of the rhenium sphere in experiment B13. Points on the flat section of the graph either side of the red line were deemed to have achieved terminal velocity, which is first reached after 30 ms. The sharp deceleration at 130 ms occurs as the sphere approaches the bottom of the capsule.

### 152 3.2. Sample Analysis

153 After the experiments, the samples were quenched and recovered for elec-  
 154 tron microprobe analysis at EMMAC (The Edinburgh Materials and Micro-  
 155 Analysis Centre), University of Edinburgh. The analyses were performed on  
 156 a CAMECA SX100 electron microprobe with a 15 kV accelerating voltage

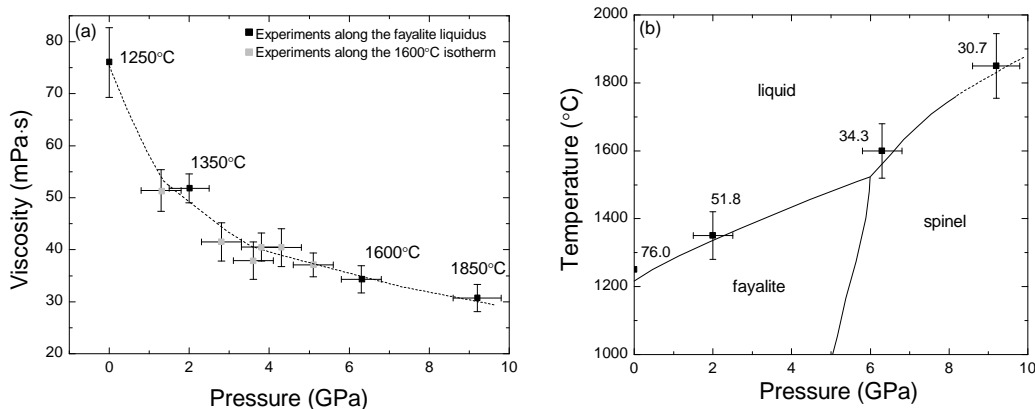


Figure 3: (a) The viscosity of liquid fayalite as a function of pressure. The black squares are values obtained along the fayalite liquidus (Run A), with the temperature indicated. The grey squares are values obtained along the 1600 °C isotherm (Run B). The ambient pressure measurement is from Shiraishi et al. (1978) at 1250 °C. The trend is a guide for the eye. (b) The  $P$ - $T$  conditions of each run obtained along the fayalite liquidus (Run A) in relation to the  $\text{Fe}_2\text{SiO}_4$  phase diagram. The viscosity values are shown in mPa·s beside each  $P$ - $T$  point.

157 and a 1  $\mu\text{m}$  beam, with a current of 30 nA. Table 2 shows the average com-  
 158 position of quenched fayalite obtained by the electron microprobe analysis.  
 159 In one of the highest  $P$  runs (A12, 6.3 GPa), a very small amount of inter-  
 160 stitial areas richer in FeO were detected. This was not the case for the other  
 161 samples (e.g. the example illustrated in Fig. 4) where only fayalite crystals  
 162 were detected. Whilst this suggests minor oxidation in the sample with FeO  
 163 in some of the interstices, we consider it to be unimportant for the following  
 164 reasons: (i) Sanloup et al. (2013a) used Mössbauer spectroscopy to quantify  
 165 the ratio of  $\text{Fe}^{3+}$  to  $\text{Fe}^{2+}$  in fayalite after high  $P$ - $T$  experiments and found no  
 166 evidence for the presence of  $\text{Fe}^{3+}$  within the experimental uncertainty ( $\sim 1\%$ )  
 167 when the same cell assembly as in the present study was used, and (ii) the  
 168 decomposition of fayalite could be tracked *in situ* upon melting as Fe-rich  
 169 blobs were apparent on the X-ray radiographs due to their strong absorption

170 contrast with the silicate melt. For the data presented here, no heterogeneity  
 171 was detected *in situ* by X-ray radiography. We did however detect a Re-Fe  
 172 alloy on the rim of some of the recovered spheres. The rims were significant,  
 173 up to 40  $\mu\text{m}$  in thickness, however we must conclude that this growth occurred  
 174 after the fall as no growth in the size of the spheres was detected during the  
 175 fall within the error of  $\pm 2 \mu\text{m}$ , and the Fe-rich rim would have been very  
 176 visible on the radiographs and this was not observed. We therefore consider  
 177 interaction between the spheres and the sample during the experiments to  
 178 be negligible.

oxide	wt%	$\delta$
SiO <sub>2</sub>	29.34	0.15
FeO	65.25	0.41
MgO	0.63	0.01
CaO	0.03	0.01
MnO	4.29	0.14
Total	99.54	

Table 2: Mean composition from 41 analyses on the quenched fayalite samples. Data is given in oxide wt% along with the standard deviation ( $\delta$ ). The sample is natural fayalite and contains approximately 4.3 wt% MnO, 0.6 wt% MgO and trace amounts of CaO.

179 A Philips XL30CP scanning electron microscope (SEM) at EMMAC and  
 180 the Institute of Petroleum Engineering, Heriot Watt University was used to  
 181 image the samples. A back scattered electron (BSE) image of experimental  
 182 run A5 is shown in Fig. 4.

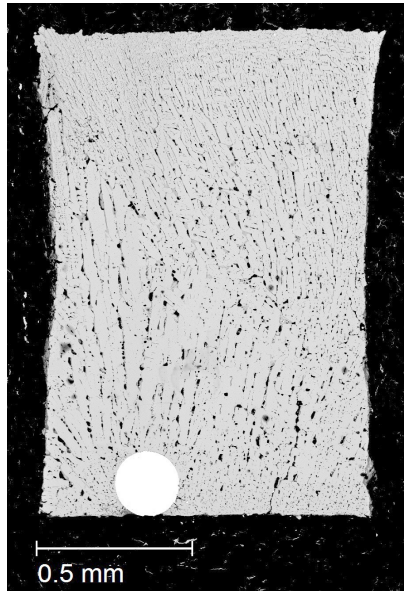


Figure 4: A BSE SEM image of experimental run A5. The sample was quenched as 100% fayalite crystals. The rhenium sphere can be seen in the bottom left side of the sample. The dark material surrounding the sample is the graphite capsule.

## 183 4. Discussion

### 184 4.1. Viscosity and structure of liquid fayalite at high pressure

185 Liquid fayalite exhibits an average Fe-O coordination number (CN) of  
186 4.8 (2) at ambient pressure which arises from the co-existence of approxi-  
187 mately 60%  $\text{FeO}_4$  and 40%  $\text{FeO}_6$  units (Drewitt et al., 2013). With increas-  
188 ing pressure up to 7.5 GPa, energy dispersive X-ray diffraction measurements  
189 show that the average Fe-O CN increases to 7.2 (3) (Sanloup et al., 2013a).  
190 However, it is not possible to determine the relative proportions of differ-  
191 ent  $\text{FeO}_x$  species as the real-space resolution of the high pressure diffraction  
192 measurements is limited. The proposed viscosity decrease in liquid fayalite  
193 is therefore likely due to the increase in Fe-O coordination with pressure.

194 This is particularly significant in the light of work that demonstrates that  
195 the  $\text{Mg}_2\text{SiO}_4$  glass structure network largely consists of  $\text{MgO}_x$  polyhedra  
196 (Kohara et al., 2004). If we assume that  $\text{Fe}_2\text{SiO}_4$  behaves in the same way,  
197 then an increase in Fe-O coordination would result in the melt structure  
198 becoming more depolymerised, thus resulting in a decrease in viscosity. In  
199 addition, higher coordinated cations are characterised by longer and thus  
200 weaker cation-oxygen bonds, which is thought to lower the activation barriers  
201 to self-diffusion, and hence leads to a further reduction in viscosity (Waff,  
202 1975; Reid et al., 2003; Liebske et al., 2005).

203 At high  $P$ , a silicate melt is expected to reach a densely packed state after  
204 which there are no further changes in cation coordination (i.e. a viscosity  
205 minimum). The viscosity minimum will vary for silicate melts of different  
206 composition. The four- to six-fold Si coordination change occurring between  
207 20-35 GPa (Sato and Funamori, 2010; Sanloup et al., 2013b) might not necessarily  
208 influence fayalite melt as it is thought to consist of isolated silica  
209 tetrahedra with a structure built from  $\text{FeO}_x$  polyhedra. Indeed, the effect of  
210 the Si coordination change is still unknown for even the most polymerised  
211 silicate melts, as viscosity experiments have so far been limited to below 13  
212 GPa. In order to complement theoretical studies, further experimental studies  
213 on silicate melts at high pressure are needed in order to fully understand  
214 the effects of the various pressure induced structural changes in relation to  
215 melt viscosity.

#### 216 *4.2. The effect of temperature on the viscosity of fayalite melt*

217 It is noteworthy that the viscosity values measured at 1600 °C are not  
218 lower than those measured at lower temperatures (within the error bars).

219 In fact, when the isotherm and liquidus viscosity values are plotted on the  
220 same diagram (Fig. 3a), the values all fit on the same trend. This suggests  
221 that at high  $T$ , temperature may have very little effect on viscosity and that  
222 pressure is the controlling variable.

223 A weak  $T$ -dependency implies that the liquid is fragile, i.e. it has a  
224 non-Arrhenian viscosity behaviour. Depolymerised silicate melts have been  
225 shown to be fragile liquids at 1 bar (Giordano et al., 2008). In fayalite  
226 melt, this fragile behaviour is reinforced at high  $P$  following its structural  
227 rearrangements. The changes that occur at high  $P$ , i.e. the increase of Fe-O  
228 CN and strengthening of the medium-range order (Sanloup et al., 2013a),  
229 are likely to further increase the liquid fragility. This effect has been shown  
230 for  $\text{SiO}_2$  and  $\text{Na}_2\text{O-SiO}_2$  melts from a computational approach (Barrat et al.,  
231 1997; Micoulaut and Bauchy, 2013), whereby the liquid goes from strong to  
232 fragile and becomes less viscous as the Si-O CN increases from 4 to 6.

#### 233 *4.3. The effect of pressure on the viscosity of silicate melts*

234 A summary of previous experimental studies on the viscosity of silicate  
235 melts is shown in Fig. 5. A viscosity decrease at high pressure has been pre-  
236 viously documented in many polymerised silicate melts e.g. jadeite (Kushiro,  
237 1976; Suzuki et al., 2011) and albite (Suzuki et al., 2002). The decrease in  
238 viscosity of polymerised melts at high pressure is much greater than in our  
239 depolymerised fayalite melt. Liquid fayalite viscosity decreased by a factor of  
240 2.5 between 0-9 GPa, whereas liquid jadeite viscosity decreased by a factor of  
241 10 between 0-2.4 GPa (Kushiro, 1976), a much smaller pressure range. Since  
242 fayalite melt is already highly depolymerised, structural changes will have a  
243 less significant effect on the melt viscosity.

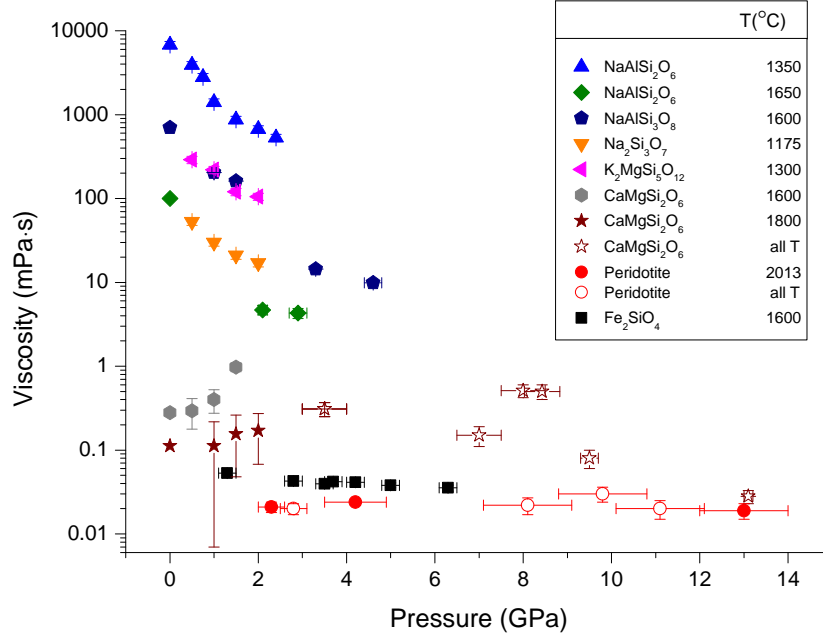


Figure 5: A summary of experimental studies on the viscosity of silicate melts. The temperature is also given for each composition. Black squares: fayalite at 1600 °C , this study; filled circles: peridotite at 2013 °C (Liebske et al., 2005); open circles: peridotite at all  $T$  (Liebske et al., 2005); blue triangles: jadeite at 1350 °C (Kushiro, 1976); green diamonds: jadeite at 1650 °C (Suzuki et al., 2011); grey hexagons: diopside at 1600 °C (Brearley et al., 1986); filled stars: diopside at 1800 °C (Taniguchi, 1992), highest pressure point from Reid et al. (2003) at  $1730 \pm 100$  °C; open stars: diopside at all  $T$  (Reid et al., 2003); navy pentagons: albite at 1600 °C, first 3 points from Brearley et al. (1986), points at 3.3 and 4.6 GPa from Suzuki et al. (2002); magenta triangles:  $K_2MgSi_5O_{12}$  at 1300 °C (Kushiro, 1977); orange triangles:  $Na_2Si_3O_7$  at 1175 °C (Kushiro, 1976).

244 Of experimentally determined viscosities, fayalite is thus far the most de-  
 245 polymerised silicate melt to have been measured. Previous studies on depoly-  
 246 merised melts (diopside (Brearley et al., 1986; Taniguchi, 1992; Reid et al.,  
 247 2003) and peridotite (Liebske et al., 2005)) found the viscosity to initially  
 248 increase with pressure, but decrease above  $\sim 9-10$  GPa. However, simula-

249 tions on liquid  $\text{MgSiO}_3$  found an anomalous pressure-dependence similar to  
250 what has been reported for polymerised melts, with the viscosity reaching a  
251 minimum value near 5 GPa, and then increasing upon further compression  
252 (Karki and Stixrude, 2010).

253 The anomalous inverse pressure-viscosity relationship of polymerised sil-  
254 icate melts has often been attributed to depolymerisation in the melt via  
255 the increase in  $\text{Al}^{3+}$  coordination with oxygen e.g. (Waff, 1975; Kushiro,  
256 1976). Particular emphasis has therefore been placed on the determination  
257 of aluminosilicate glass structure at high pressure. Allwardt et al. (2007)  
258 reported the significant presence of 5-fold coordinated aluminium in a range  
259 of aluminosilicate glasses at 3 GPa, however the relative proportions of the  
260 4-,5- and 6-fold coordinated Al was highly variable between glasses of dif-  
261 ferent compositions. On the other hand, Poe et al. (2001) found no signif-  
262 icant changes in Al coordination below 6 GPa. Other explanations for the  
263 anomalous viscosity behaviour of silicate melts include the negative thermal  
264 expansion coefficient of the liquid (Schmelzer et al., 2005) and a reactive  
265 ion transfer model, whereby the  $\text{O}^{2-}$  self-diffusivity increases with increas-  
266 ing pressure, resulting in a viscosity decrease (McMillan and Wilding, 2009).  
267 However, a recent theoretical study by Bauchy et al. (2013) attempted to re-  
268 late viscosity and diffusivity of silicate melts at high pressure, but could not  
269 find a definitive relationship. The clear discrepancies in the literature, com-  
270 bined with the additional problem that high pressure Si-O and Al-O bond  
271 arrangements have been found to return to tetrahedral coordination upon  
272 decompression (Williams and Jeanloz, 1988), demonstrate the need for the  
273 *in situ* determination of the structure of silicate melts. The experimental

274 difficulties associated with the *in situ* determination of liquid structures has  
275 resulted in very few studies possessing both viscosity and *in situ* structural  
276 data. Exceptions include the present study and Sakamaki et al. (2013), who  
277 measured the viscosity and structure of basaltic magma.

278 Our results show that cations other than  $\text{Al}^{3+}$  experience coordination  
279 changes over the 0-10 GPa pressure range. It is likely, on the basis that  
280 molten fayalite exhibits different behaviour to other depolymerised melts  
281 such as diopside and peridotite, that a catch-all theory for the behaviour of  
282 depolymerised silicate melts at depth is not appropriate. Behaviour should  
283 be considered on an individual basis and may be strongly dependent on the  
284 melt structure and composition.

#### 285 4.4. Geological Implications

286 Our results hold particular significance for FeO-rich planetary magmas  
287 existing in reduced environments. Our experiments were carried out under  
288 reducing conditions and the final sample composition was found to contain  
289  $\text{Fe}^{3+}/\sum \text{Fe} \leq 0.01$  (Sanloup et al., 2013a). The present day Moon and  
290 Mars are estimated to have high-mantle iron contents (up to 22 wt% FeO  
291 (Cahill et al., 2009; Baratoux et al., 2011)) in a reducing environment (Sato  
292 et al., 1973; Herd et al., 2002).  $fO_2$  has been found to have an effect on  
293 melt viscosity e.g. Liebske et al. (2003); Bouhifd et al. (2004); Chevrel et al.  
294 (2014) all found a drop in silicate melt viscosity with a reduction in  $\text{Fe}^{3+}/\sum$   
295 Fe.

296 Lacks et al. (2007) carried out molecular dynamics simulations to calcu-  
297 late viscosity along the MgO-SiO<sub>2</sub> join to investigate the effect of composition  
298 and pressure on transport properties. At atmospheric pressure, viscosity was

299 found to vary by more than 3 orders of magnitude along the compositional  
300 join, however at pressures  $> 15$  GPa, the viscosity varied by less than an  
301 order of magnitude over the entire compositional range. If the FeO-SiO<sub>2</sub>  
302 system behaves in the same way, then planetary magma viscosities will be  
303 particularly sensitive to FeO content at lower pressures. Our results suggest  
304 that the increase in  $P$  along the magma ocean adiabat will favour a decrease  
305 in melt viscosity of a FeO-rich magma, and may be most important at upper  
306 mantle depths. Additionally, the viscosity decrease may be particularly pro-  
307 nounced in more reducing conditions, such as those considered to be present  
308 in Mars and the Moon. Bodies that are less FeO rich (such as Mercury) may  
309 have a less pronounced negative pressure effect (or it may not be present at  
310 all) and it is therefore worth considering when modelling processes occurring  
311 in planetary magma oceans.

312 Due to the lack of data on silicate melts at high pressure, assumptions  
313 about the viscosity of depolymerised melts at depth have often been made.  
314 Solomatov and Stevenson (1993) assumed that the viscosity of depolymerised  
315 melts would increase with depth due to closer interatomic spacing. Tonks  
316 and Melosh (1990, 1993) assumed no pressure effect on silicate melt viscosity  
317 in their global magma ocean model. Our results however, show that depoly-  
318 merised silicate melts may exhibit a hitherto unexpected decrease in viscosity  
319 at depth. Viscosity will have been an important influencing property on the  
320 chemical evolution of the early terrestrial bodies due to the fact that convec-  
321 tion (Davaille and Jaupart, 1993), crystal settling (Solomatov and Stevenson,  
322 1993), cumulate overturn (Elkins-Tanton et al., 2003), and chemical diffusion  
323 (Rubie et al., 2003) are much more efficient in low viscosity melts. However,

324 more work is needed to understand the properties of other silicate melts rel-  
325 evant to magma ocean compositions across a larger pressure range. Whilst  
326 the existence of a fayalitic magma ocean in a planetary body is unlikely, it  
327 is nevertheless important to measure the properties of simple end-member  
328 compositions so that we can begin to understand how different compositional  
329 mixtures influence planetary magma viscosity and processes.

## 330 5. Conclusions

331 *In situ* falling sphere viscometry was performed on liquid fayalite ( $\text{Fe}_2\text{SiO}_4$ ),  
332 a highly depolymerised, Fe-rich silicate melt, up to 9.2 GPa and  $\sim 1850^\circ\text{C}$ .  
333 This is the most depolymerised silicate melt studied so far, and the viscosity  
334 was found to decrease by a factor of 2.5 over the measured pressure range.  
335 It is likely that this decrease is a result of the increase in Fe-O coordination  
336 with pressure (Sanloup et al., 2013a). In polymerised melts, the structural  
337 transformation of tetrahedrally coordinated cations (such as  $\text{Al}^{3+}$ ) to higher  
338 species has often been cited as the cause of the anomalous viscosity behaviour  
339 of silicate melts. Hitherto, it has often been assumed that depolymerised sil-  
340 icate melts will not exhibit anomalous viscosity behaviour at depth. Our  
341 results show that this assumption is not appropriate, and that the behaviour  
342 of silicate melts at depth should be considered on an independent basis for  
343 melts of different composition. This has important implications for models  
344 of planetary differentiation. In particular, terrestrial bodies with high Fe  
345 contents and reducing mantle conditions are likely to have had very mobile  
346 melts at depth.

347 **Acknowledgments**

348 We thank C. Kenney-Benson for providing cell-assembly parts, J.W.E.  
349 Drewitt for his assistance with data acquisition, electron microprobe analy-  
350 ses and useful discussions during preparation of the manuscript, C. Hayward  
351 for his help with electron microprobe analyses and R. Askew and J. Buckman  
352 for their assistance with the scanning electron microscope. High-pressure ex-  
353 periments were performed at HPCAT (Sector 16), Advanced Photon Source  
354 (APS), Argonne National Laboratory. HPCAT operations are supported by  
355 DOE-NNSA under Award No. DE-NA0001974 and DOE-BES under Award  
356 No. DE-FG02-99ER45775, with partial instrumentation funding by NSF.  
357 APS is supported by DOE-BES, under Contract No. DE-AC02-06CH11357.  
358 This work was supported by the Engineering and Physical Sciences Research  
359 Council and the European Research Council under the European Commu-  
360 nity's Seventh Framework Programme (FP7/20072013 Grant Agreement No.  
361 259649 to C.S.).

362 Agee, C. B., 1992. Isothermal compression of molten  $\text{Fe}_2\text{SiO}_4$ . *Geophysical*  
363 *Research Letters* 19, 1169–1172.

364 Allwardt, J. R., Stebbins, J. F., Terasaki, H., Du, L., Frost, D. J., Withers,  
365 A. C., Hirschmann, M. M., Suzuki, A., E., O., 2007. Effect of structural  
366 transitions on properties of high-pressure silicate melts:  $^{27}\text{Al}$  NMR, glass  
367 densities, and melt viscosities. *American Mineralogist* 92, 1093–1104.

368 Baratoux, D., Toplis, M. J., Monnereau, M., Gasnault, O., 2011. Thermal  
369 history of Mars inferred from orbital geochemistry of volcanic provinces.  
370 *Nature* 472, 338–342.

- 371 Barrat, J., Badro, J., Gillet, P., 1997. A strong to fragile transition in a  
372 model of liquid silica. *Molecular Simulation* 20, 17–25.
- 373 Bauchy, M., Guillot, B., Micoulaut, M., Sator, N., 2013. Viscosity and viscos-  
374 ity anomalies of model silicates and magmas: A numerical investigation.  
375 *Chemical Geology* 346, 47–56.
- 376 Bouhifd, M. A., Richet, P., Besson, P., Roskosz, M., Ingrin, J., 2004. Redox  
377 state, microstructure and viscosity of a partially crystallized basalt melt.  
378 *Earth and Planetary Science Letters* 218, 31–44.
- 379 Brearley, M., Dickinson, J. E., Scarfe, C., 1986. Pressure dependence of melt  
380 viscosities on the join diopside-albite. *Geochimica et Cosmochimica Acta*  
381 50, 2563–2570.
- 382 Brizard, M., Megharfi, M., Verdier, C., 2005. Absolute falling-ball viscometer:  
383 evaluation of measurement uncertainty. *Metrologia* 42, 298–303.
- 384 Cahill, J. T. S., Lucey, P. G., Wieczorek, M. A., 2009. Compositional varia-  
385 tions of the lunar crust: results from radiative transfer modeling of central  
386 peak spectra. *Journal of Geophysical Research* 114, E09001.
- 387 Chen, G. Q., Ahrens, T. J., Stolper, E. M., 2002. Shock-wave equation of  
388 state of molten and solid fayalite. *Physics of the Earth and Planetary*  
389 *Interiors* 134, 35–52.
- 390 Chevrel, M. O., Baratoux, D., Hess, K., Dingwell, D. B., 2014. Viscous flow  
391 behavior of tholeiitic and alkaline fe-rich martian basalts. *Geochimica et*  
392 *Cosmochimica Acta* 124, 348–365.

- 393 Davaille, A., Jaupart, C., 1993. Thermal convection in lava lakes. *Geophysical*  
394 *Research Letters* 20, 1827–1830.
- 395 Elkins-Tanton, L. T., Parmentier, E. M., Hess, P. C., 2003. Magma ocean  
396 fractional crystallization and cumulate overturn in terrestrial planets: Im-  
397 plications for Mars. *Meteoritics and Planetary Science* 38, 1753–1771.
- 398 Faxén, H., 1922. Der widerstand gegen die bewegung einer starren kugel  
399 in einer zähen flüssigkeit, die zwischen zwei parallelen ebenen wänden  
400 eingeschlossen ist. *Annalen der Physik* 373, 89–119.
- 401 Ghosh, D., Karki, B., 2011. Diffusion and viscosity of  $\text{Mg}_2\text{SiO}_4$  liquid at high  
402 pressure from first-principles simulations. *Geochimica et Cosmochimica*  
403 *Acta* 75, 4591–4600.
- 404 Giordano, D., Russell, J. K., Dingwell, D. B., 2008. Viscosity of magmatic  
405 liquids: A model. *Earth and Planetary Science Letters* 271, 123–134.
- 406 Herd, C. D. K., Borg, L. E., Jones, J. H., Papike, J. J., 2002. Oxygen fugacity  
407 and geochemical variations in the martian basalts: implications for martian  
408 basalt petrogenesis and the oxidation state of the upper mantle of Mars.  
409 *Geochimica et Cosmochimica Acta* 66, 2025–2036.
- 410 Karki, B. B., Stixrude, L. P., 2010. Viscosity of  $\text{MgSiO}_3$  at Earth’s mantle  
411 conditions: implications for an early magma ocean. *Science* 328, 740–742.
- 412 Kerr, R. C., Lister, J. R., 1991. The effects of shape on crystal settling and  
413 on the rheology of magmas. *The Journal of Geology* 99, 457–467.

- 414 Kohara, S., Suzuya, K., Takeuchi, K., Loong, C. K., Grimsditch, M., Weber,  
415 J. K. R., Tangeman, J. A., Key, T. S., 2004. Glass formation at the limit  
416 of insufficient network formers. *Science* 303, 1649–1652.
- 417 Kono, Y., Irifune, T., Higo, Y., Inoue, T., Barnhoorn, A., 2010. *P-V-T*  
418 relation of MgO derived by simultaneous elastic wave velocity and in situ  
419 X-ray measurements: A new pressure scale for the mantle transition region.  
420 *Physics of the Earth and Planetary Interiors* 183, 196–211.
- 421 Kono, Y., Kenney-Benson, C., Park, C., Shen, G., Wang, Y., 2013. Anomaly  
422 in the viscosity of liquid KCl at high pressures. *Physical Review B* 87,  
423 024302.
- 424 Kono, Y., Park, C., Kenney-Benson, C., Shen, G., Wang, Y., 2014. Toward  
425 comprehensive studies of liquids at high pressures and high temperatures:  
426 Combined structure, elastic wave velocity, and viscosity measurements in  
427 the Paris Edinburg cell. *Physics of the Earth and Planetary Interiors* 228,  
428 269–280.
- 429 Kushiro, I., 1976. Changes in viscosity and structure of melt of  $\text{NaAlSi}_2\text{O}_6$   
430 composition at high pressures. *Journal of Geophysical Research* 81, 6347–  
431 6350.
- 432 Kushiro, I., 1977. Phase transformation in silicate melts under upper mantle  
433 conditions. In: M.H. Manghnani and S. Akimoto (Ed.), *High-Pressure*  
434 *Research Applications in Geophysics*. Academic, pp. 25–37.
- 435 Kushiro, I., Yoder, H. S., Mysen, B. O., 1976. Viscosities of basalt and an-

- 436 desite melts at high pressures. *Journal of Geophysical Research* 81, 6351–  
437 6356.
- 438 Lacks, D. J., Rear, D. B., Van Orman, J. A., 2007. Molecular dynamics  
439 investigation of viscosity, chemical diffusivities and partial molar volumes  
440 of liquids along the MgO–SiO<sub>2</sub> join as functions of pressure. *Geochimica  
441 et Cosmochimica Acta* 71, 1312–1323.
- 442 Liebske, C., Behrens, H., Holtz, F., Lange, R. A., 2003. The influence of  
443 pressure and composition on the viscosity of andesitic melts. *Geochimica  
444 et Cosmochimica Acta* 67, 473–485.
- 445 Liebske, C., Schmickler, B., Terasaki, H., Poe, B. T., Suzuki, A., Funakoshi,  
446 K., Ando, R., Rubie, D. C., 2005. Viscosity of peridotite liquid up to  
447 13 GPa: Implications for magma ocean viscosities. *Earth and Planetary  
448 Science Letters* 240, 589–604.
- 449 McMillan, P. F., Wilding, M. C., 2009. High pressure effects on liquid viscos-  
450 ity and glass transition behaviour, polyamorphic phase transitions and  
451 structural properties of glasses and liquids. *Journal of Non-Crystalline  
452 Solids* 355, 722–732.
- 453 Micoulaut, M., Bauchy, M., 2013. Anomalies of the first sharp diffraction  
454 peak in network glasses: Evidence for correlations with dynamic and rigid-  
455 ity properties. *Physica Status Solidi B* 250, 976–982.
- 456 Poe, B. T., Romano, C., Zotov, N., Cibin, G., Marcelli, A., 2001. Com-  
457 pression mechanisms in aluminosilicate melts: Raman and XANES spec-

- 458     troscopy of glasses quenched from pressures up to 10 GPa. *Chemical Ge-*  
459     *ology* 174, 21–31.
- 460 Reid, J. E., Suzuki, A., Funakoshi, K., Terasaki, H., Poe, B. T., Rubie, D. C.,  
461     Ohtani, E., 2003. The viscosity of  $\text{CaMgSi}_2\text{O}_6$  liquid at pressures up to 13  
462     GPa. *Physics of the Earth and Planetary Interiors* 139, 45–54.
- 463 Robinson, M. S., Taylor, G. J., 2001. Ferrous oxide in Mercury’s crust and  
464     mantle. *Meteoritics and Planetary Science* 36, 841–847.
- 465 Rubie, D. C., Melosh, H. J., Reid, J. E., Liebske, C., Righter, K., 2003.  
466     Mechanisms of metal-silicate equilibration in the terrestrial magma ocean.  
467     *Earth and Planetary Science Letters* 205, 239–255.
- 468 Sakamaki, T., Suzuki, A., Ohtani, E., Terasaki, H., Urakawa, S., Katayama,  
469     Y., Funakoshi, K., Wang, Y., Hernlund, J. W., Ballmer, M. D., 2013.  
470     Ponded melt at the boundary between the lithosphere and asthenosphere.  
471     *Nature Geoscience* 6, 1041–1044.
- 472 Sakamaki, T., Wang, Y., Park, C., Yu, T., Shen, G., 2012. Structure of  
473     jadeite melt at high pressures up to 4.9 GPa. *Journal of Applied Physics*  
474     111, 112623.
- 475 Sanloup, C., Drewitt, J. W. E., Crépisson, C., Kono, Y., Park, C., McCam-  
476     mon, C., Hennem, L., Brassamin, S., Bychkov, A., 2013a. Structure and  
477     density of molten fayalite at high pressure. *Geochimica et Cosmochimica*  
478     *Acta* 118, 118–128.

- 479 Sanloup, C., Drewitt, J. W. E., Konôpková, Z., Dalladay-Simpson, P., Mor-  
480 ton, D. M., Rai, N., van Westrenen, W., Morgenroth, W., 2013b. Structural  
481 change in molten basalt at deep mantle conditions. *Nature* 503, 104–107.
- 482 Sato, M., Hickling, N. L., McLane, J. E., 1973. Oxygen fugacity values of  
483 Apollo 12, 14 and 15 lunar samples and reduced state of lunar magmas.  
484 *Proceedings of the Lunar Science Conference* 4, 1061–1079.
- 485 Sato, T., Funamori, N., 2010. High-pressure structural transformation of  
486 SiO<sub>2</sub> glass up to 100 GPa. *Physical Review B* 82, 184102.
- 487 Schmelzer, J. W. P., Zanutto, E. D., Fokin, V. M., 2005. Pressure dependence  
488 of viscosity. *The Journal of Chemical Physics* 122, 074511.
- 489 Shiraishi, Y. K., Ikeda, K., Tamura, A., Saitô, T., 1978. On the viscosity  
490 and density of the molten FeO–SiO<sub>2</sub> system. *Transactions of the Japan*  
491 *Institute of Metals* 19, 264–274.
- 492 Solomatov, V., Stevenson, D., 1993. Suspension in convective layers and  
493 style of differentiation of a terrestrial magma ocean. *Journal of geophysical*  
494 *Research* 98, 5375–5390.
- 495 Suzuki, A., Ohtani, E., Funakoshi, K., Terasaki, H., Kubo, T., 2002. Viscosity  
496 of albite melt at high pressure and temperature. *Physics of Chemistry and*  
497 *Minerals* 29, 159–165.
- 498 Suzuki, A., Ohtani, E., Terasaki, H., Nishida, K., Hayashi, H., Sakamaki, T.,  
499 Shibazaki, Y., Kikegawa, T., 2011. Pressure and temperature dependence  
500 of the viscosity of a NaAlSi<sub>2</sub>O<sub>6</sub> melt. *Physics and Chemistry of Minerals*  
501 38, 59–64.

- 502 Taniguchi, H., 1992. Entropy dependence of viscosity and the glass-transition  
503 temperature of melts in the system diopside-anorthite. *Contributions to*  
504 *Mineralogy and Petrology* 109, 295–303.
- 505 Thomas, C. W., Liu, Q., Agee, C. B., Asimow, P. D., Lange, R. A., 2012.  
506 Multi-technique equation of state for  $\text{Fe}_2\text{SiO}_4$  melt and the density of Fe-  
507 bearing silicate melts from 0 to 161 GPa. *Journal of Geophysical Research:*  
508 *Solid Earth* 117, B10206.
- 509 Tonks, W. B., Melosh, H. J., 1990. The physics of crystal settling and suspen-  
510 sion in a turbulent magma ocean. In: N.E. Newsom and J.H. Jones (Ed.),  
511 *Origin of the Earth*. Oxford University Press, New York, pp. 151–174.
- 512 Tonks, W. B., Melosh, H. J., 1993. Magma ocean formation due to giant  
513 impacts. *Journal of geophysical Research* 98, 5319–5333.
- 514 Vohra, Y. K., Duclos, S. J., Ruoff, A. L., 1987. High-pressure x-ray diffraction  
515 studies on rhenium up to 216 GPa (2.16 Mbar). *Physical Review B* 36,  
516 9790–9792.
- 517 Waff, H. S., 1975. Pressure-induced coordination changes in magmatic liq-  
518 uids. *Geophysical Research Letters* 2, 193–196.
- 519 Williams, Q., Jeanloz, R., 1988. Spectroscopic evidence for pressure-induced  
520 coordination changes in silicate glasses and melts. *Science* 239, 902–905.